Mass Spectroscopic Observation of Shock-Induced Chemistry in Liquid CS_2

Ray Engelke,* Normand C. Blais, and Stephen A. Sheffield

MS P952, Los Alamos National Laboratory, Los Alamos, New Mexico 87545

Received: September 26, 2007; In Final Form: October 11, 2007

We have observed, via time-of-flight mass spectrometry, 13 chemical species more massive than CS_2 produced by shocking liquid CS_2 to very high pressure/temperature. The stoichiometry of three of these species is uniquely determined from the $^{12}CS_2$ experiments; these species are C_2S_2, C_3S_2, and C_4S_2. The stoichiometry of the other 10 structures cannot be uniquely determined from $^{12}CS_2$ experiments. However, by redoing the experiments using isotopically labeled CS_2 (i.e., $^{13}CS_2$), we determined the stoichiometry of nine of the remaining structures. The nine structures are S_n ($n = 3-8$) and CS_3, C_2S_5, and C_4S_6. A structure with mass 297.1 amu was also observed in the $^{12}CS_2$ experiments but was not detected in the $^{13}CS_2$ experiments. This structure must be C_6S_7, $C_{14}S_4$, or $C_{22}S$; given the low carbon content of the other observed carbon species, it is probably C_6S_7. The shockwaves to which the CS_2 molecules were subjected were produced by the detonation of high mass-density solid explosives. The explosives used were either a plastic bonded form of cyclotetramethylene tetranitramine or pure hexanitrostilbene. Numerical compressible fluid−mechanical simulations were done to estimate the pressures, temperatures, and time scales of the processes that occurred in the shocked CS_2. The results obtained in the present experiments are related to earlier work on CS_2's chemical reactivity that used both shockwave methods and static techniques to produce very high pressure.

I. Introduction

Bridgman was the first worker to give evidence that high pressure can produce chemical reactions in CS_2.[1] He used static high-pressure techniques and found that, after pressurization, a black substance can be recovered and studied at ambient conditions. This material is now called "Bridgman black". Whalley,[2] via infrared absorption studies of the black material, gave evidence that it is a linear polymer of the form $[SC{=}S]_n$.

The first thorough study of CS_2 that used shockwave techniques is due to R. D. Dick.[3,4] Later, experiments were done by Sheffield[5] for the purpose of studying the shock-induced reaction that was evidenced by a cusp in CS_2's Hugoniot. Additional experiments were done for the purpose of establishing the onset of chemical reaction.[6] The pressure−volume Hugoniot data from these three studies are shown in Figure 1; notice the cusps at ca. 50 and 80 kbar. In this pressure region, the material becomes more compressible and undergoes a volume reduction of ca. 26%. This "collapse" indicates that higher molecular weight structures are being produced by the shock process. Dick speculated that above 80 kbar a complete transformation of the liquid CS_2 to Bridgman black has occurred. No further cusps were observed on the CS_2 Hugoniot up to Dick's maximum pressure input of 526 kbar.

Dick's experiments were all explosively driven. The study by Sheffield[5] used gas-gun-driven shock inputs to the CS_2 with the initial shock reflecting off a single-crystal sapphire back plate to produce pressures high enough to induce a chemical reaction. Hugoniot points below the onset of reaction were measured and are shown in Figure 1. Because the input shocks to the CS_2 were double shocks (the input shock and then a reflected shock from the sapphire), the reaction varied in such a fashion that it appeared more effected by temperature than by pressure. To estimate the temperature, complete equations of state were developed for both the CS_2 and the reaction products, based on the measured Hugoniot data available.[7] While

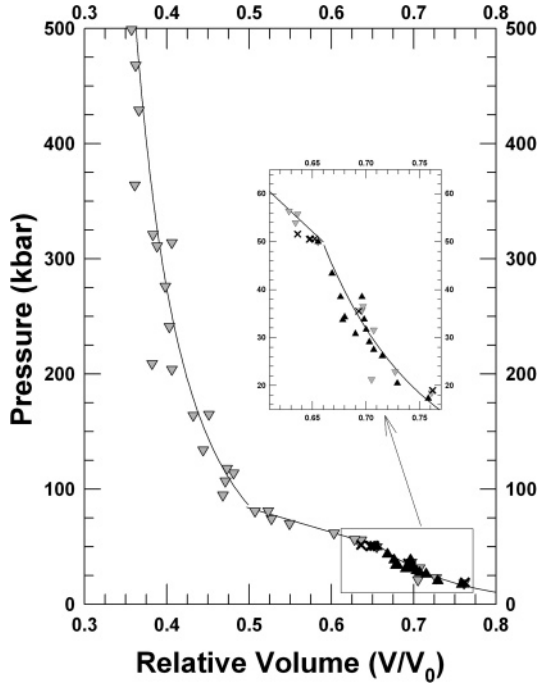

Figure 1. Pressure−volume Hugoniot for CS_2 based on data by Dick[3,4] and Sheffield.[5,6] A discussion of the difference in Dick's data between refs 3 and 4 is contained in Appendix B of ref 5. The gray upside-down triangles are from Dick,[3] the black triangles are from Sheffield,[5] and the ×'s are from Sheffield.[6]

Dick estimated that the lower pressure cusp occurs at 62 kbar, the experiments of Sheffield and Duvall led to a revised estimate of 50 ± 4 kbar. Further gas-gun experiments of Sheffield[6] have established that the onset of reaction occurs at a shock state of 51.0 ± 0.5 kbar. The insert in Figure 1 shows the data near the lower pressure cusp.

10.1021/jp0777364 CCC: $40.75
Published on Web 12/06/2007

In the present work, we used the LANL detonation chemistry apparatus (DCA)[8] to determine the stoichiometry of 13 molecules more massive than CS_2, produced by strongly shocking liquid CS_2. The DCA is an instrument in which small quantities of high explosive can be detonated. The shockwaves generated by detonating explosives were used to drive shocks into the CS_2. A small portion of the shocked CS_2 can be introduced into a time-of-flight (TOF) mass spectrometer contained within the vacuum chamber of the DCA. Our experiments show that the early time shock-induced chemistry produces the structures S_n ($n = 3-8$), C_nS_2 ($n = 2, 3, 4$), CS_3, C_2S_5, and C_4S_6. One other structure with mass 297.1 amu was observed, but we are unable to determine its atomic composition uniquely; it is probably C_6S_7.

Compressible fluid−mechanical calculations were performed with the Sandia National Laboratories CTH computer code[9] to define the pressure/temperature histories experienced by the shocked CS_2. The calculations also provide estimates of the time scales involved in the experiments.

A more thorough discussion of the relationship between the results of earlier workers and our results will be given in the Discussion and Conclusions section of this paper.

The remainder of this paper is arranged as follows: sections II, III, IV, and V are, respectively, descriptions of (1) the experiments, (2) the results, (3) the CTH calculations, and, finally, (4) a discussion and conclusions section.

II. Experimental Aspects

Our observations were made with the LANL DCA; this apparatus has been described in detail elsewhere.[8] It is a TOF mass spectrometer with sufficient size and differential pumping to directly sample the gaseous products of detonation of small samples of explosive or of samples of material shocked by detonating explosives.

The apparatus and the procedures used to study CS_2 were similar to those used in work previously reported.[10,11] The apparatus is designed to extract the products from a reaction volume and to direct them rapidly via a molecular beam into a mass spectrometer for analysis before these products can be modified by collisions with surfaces or other molecules in the beam. It consists of four vacuum chambers, each separately pumped and connected to each other along an axis to form a straight line between the reaction volume exit and the mass spectrometer. By design, the volumes of each chamber, the connection to the adjacent chambers, the pumping speeds of the pumps, and the rapidity of the reactions studied make this possible. While the mass spectrum is being taken, the highest pressure in any of the chambers is such that the mean free path for the molecules in the beam is ca. 20 m. At most, 4% of the molecules in the beam are scattered by the background gas.

The mass spectrometer detector has modest mass resolution; the signal intensity for equal-intensity mass peaks one mass unit apart drops to about 20% at mass 150. We can locate the mass peaks to within ca. 0.2 amu for masses in the mass region between the two mass values used to calibrate the mass vs time relationship. Outside this region, the estimated mass value errors can be larger. The instrument has an additional feature: because we have two microchannel plate detectors separated in space, we can differentiate between ion signals generated from the beam at an early scan from higher mass ions generated at a previous scan.

An important aspect of our instrument is that it cannot detect ionic species produced in the reaction volume. Such species are deflected into the walls of the instrument before they can

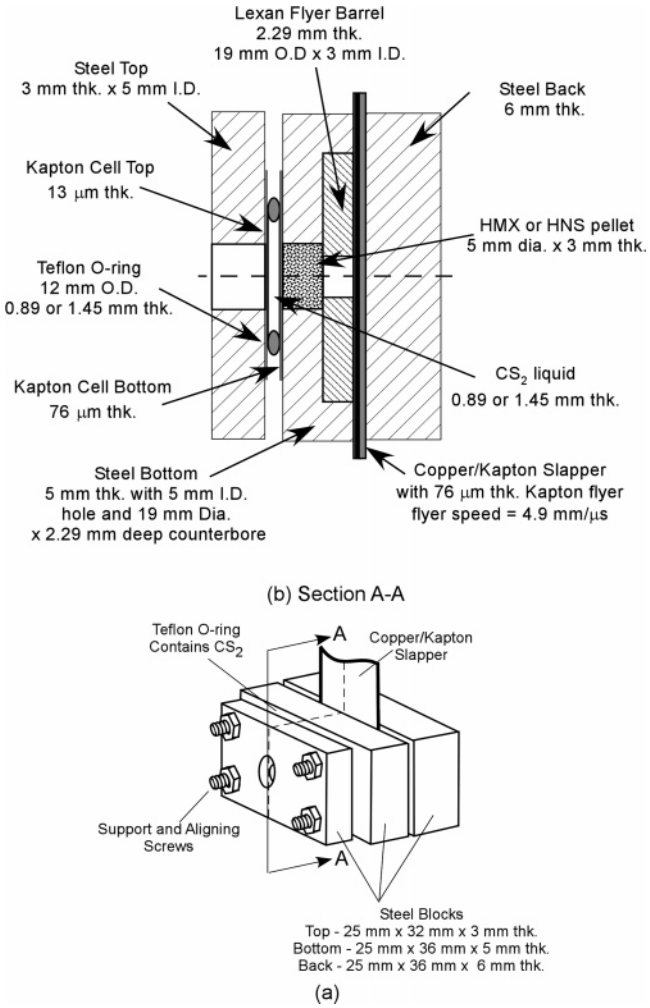

Figure 2. Schema of the assembly used in the CS_2 shockwave experiments. Figure 2a shows the assembly of the CS_2 cell on the slapper/back plate assembly. The two front pieces were screwed together as shown and then attached to the slapper/back plate by epoxy. A section has been made through the cell and is shown in Figure 2b. This shows the details of the cell construction with the CS_2 being confined by Kapton layers and a Teflon O-ring.

reach the mass spectrometer detectors. The species we observe are electrically neutral molecules from the reaction volume. These molecules are ionized by a 5-milli-amp 90-eV electron beam that intersects the neutral molecular beam for 1 μs every 12 μs (i.e., ca. 8.3% of the time).

We fired small pellets of pressed plastic-bonded cyclotetramethylene tetranitramine (HMX) or pure-pressed hexanitrostilbene (HNS), fastened to a "slapper-barrel" detonator assembly, mounted inside the high vacuum chamber of the spectrometer. The shock induced into the end of a pellet by the slapper traveling 4.9 mm/μs is strong enough to detonate the explosive (see Figure 2).

The shockwave produced by the detonating pellet moves through the Kapton layer and into the CS_2 sample. The expansion of the CS_2 gases as they exit the sample cell is rapid enough to significantly collapse the particle speed distribution, especially for those particles directed close to the symmetry axis of the flow. For these, the flow becomes effectively collisionless. By "skimming off" any particles not having these characteristics, we form a molecular beam directed into the mass spectrometer. Recording the data is completed before sufficient wall collisions of the "discarded" particles occur in the detonation chamber, which raises the pressure to affect the beam

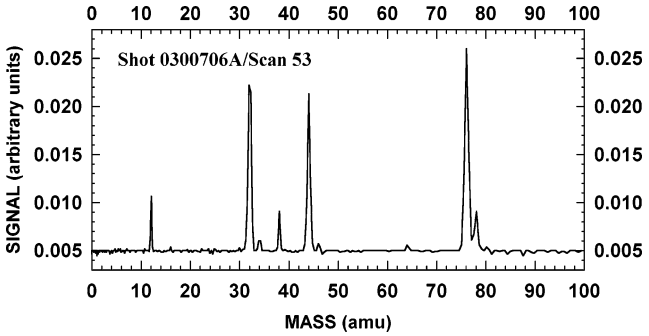

Figure 3. Fragmentation pattern obtained by shocking liquid CS_2 with 1.60 mass density HNS. This pattern is identical to the NIST pattern obtained by evaporating the CS_2 rather than shocking it. The peak at 38 amu is due to CS_2^{++}.

formation. A mass spectrum ranging from $m = 0$ to $m = 296$ amu is taken every 12 μs. This allows us to examine the change in the chemical composition of the products from successive layers of the shocked CS_2 as they arrive at the detectors of the spectrometer. In a 12-μs scan, 6000 intensity points are recorded at 2-ns intervals. In all, 100 12-μs scans are recorded.

A number of experimental sample cell configurations for the experiments were tried out before we arrived at the one used in the experiments reported here. The main difficulty with the earlier configurations was retaining the volatile liquid CS_2 sample within the assembly when the sample was in the vacuum chamber of the DCA. With the sample cell shown in Figure 2, we found that we could contain the CS_2 in a high vacuum chamber for several hours without developing bubbles in the central region of the sample. This was of critical importance since the presence of bubbles would create a three-dimensional flow when the high-pressure shockwave passed over them. Since the numerical fluid−mechanical computer calculations used to simulate the flow were done in two-dimensional cylindrical symmetry, it was critical to avoid this.

The length of the cell is such that the chemical reactions occur in regions where the particle speed along the cell symmetry axis is large compared to the lateral expansion speed when the shocked sample exits the cell. We used two different explosive materials (HMX and HNS) to change the pressure/temperature conditions to which the CS_2 sample was exposed.

CS_2 is a clear liquid at ambient conditions with mass density of 1.266 g/cm^3. It is highly volatile and penetrates easily into the structure of most flexible sealant materials. We found that Kapton film and solid Teflon worked well to form the boundaries of the CS_2 sample (see Figure 2). The $^{12}CS_2$ and $^{13}CS_2$ were used as obtained from Aldrich. They were 99+% pure CS_2. The ^{13}C content of the $^{13}CS_2$ was greater than 99%.

III. Results

Figure 3 is a fragmentation pattern of $^{12}CS_2$ obtained by shocking the material with the shock from a detonating 5 mm × 3 mm cylindrical pellet of HNS; the initial density of HNS was 1.60 g/cm^3. The raw data has been subjected to a 20-point running average in order to smooth it. The fragmentation pattern shown on the figure is essentially identical to that obtained by evaporation of the CS_2 rather than by shocking it; see, e.g., the NIST compendium[12] of fragmentation patterns.

The pattern obtained by shocking with HNS is of interest because the HNS shock produces a pressure above the cusps on the CS_2 Hugoniot. However, the time that the CS_2 is held at high pressure and temperature is short and varies as the wave moves through the liquid. The shock front attenuates as the wave

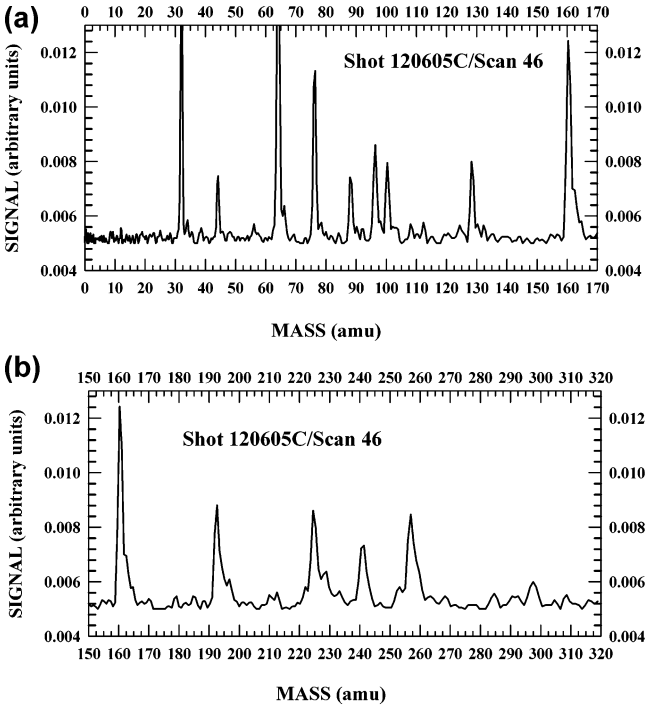

Figure 4. (a) Fragmentation pattern of the chemically reacted liquid $^{12}CS_2$ obtained by shocking the material with 1.80 mass density HMX for the mass range 0−170 amu. (b) Fragmentation pattern of the chemically reacted liquid $^{12}CS_2$ obtained by shocking the material with 1.80 mass density HMX for the mass range 150−320 amu.

travels because of the rarefaction following the explosively driven shock. Evidently the chemical kinetics that occurs in the shocked CS_2 are too slow for heavier species to form in recordable quantities when the material is shocked by a detonating HNS pellet. To increase the reaction speed, we used the higher performance explosive PBX-9501. PBX-9501 is an HMX-based plastic-bonded explosive; our pellets had a mass density of 1.80 g/cm^3. The cylindrical HNS and PBX-9501 pellets could be used interchangeably in the sample assembly.

Parts a and b of Figure 4 show a mass spectrum obtained from shocking $^{12}CS_2$ with a 5 mm × 3 mm pellet of HMX (initial mass density of 1.80 g/cm^3).

A 20-point running average has been used to smooth the raw data. Note that, for masses ≤76 amu, the same masses appear as appeared on the fragmentation pattern of CS_2 (see Figure 3); however, the relative intensities are changed. The most interesting feature of Figure 4a is the five new peaks with masses ≥76 amu. Figure 4a only displays masses up to 170 amu. Figure 4b shows the results for masses greater than 150 amu and out to 320 amu. There are six new masses in this mass range.

In other experiments, we have also seen clear evidence for masses at 108, 112, and 184 amu; these species do not show up clearly on the shot used to produce parts a and b of Figure 4. The left column of Table 1 shows the measured values of the $^{12}CS_2$ compositions seen in the experiments.

The second column of Table 1 shows the possible atomic composition of the species observed in the $^{12}CS_2$ experiments. Note that for masses 88.2, 100.4, and 112.3 the only possible structures are C_2S_2, C_3S_2, and C_4S_2, respectively. For the 10 other structures, 2 or 3 atomic compositions are possible.

To remove this ambiguity, the same type of experiments were done with $^{13}CS_2$. The results of one such experiment are shown in parts a and b of Figure 5, and the observed numerical values are given in column 3 of Table 1. These results produce unique atomic compositions for nine of the remaining peaks.

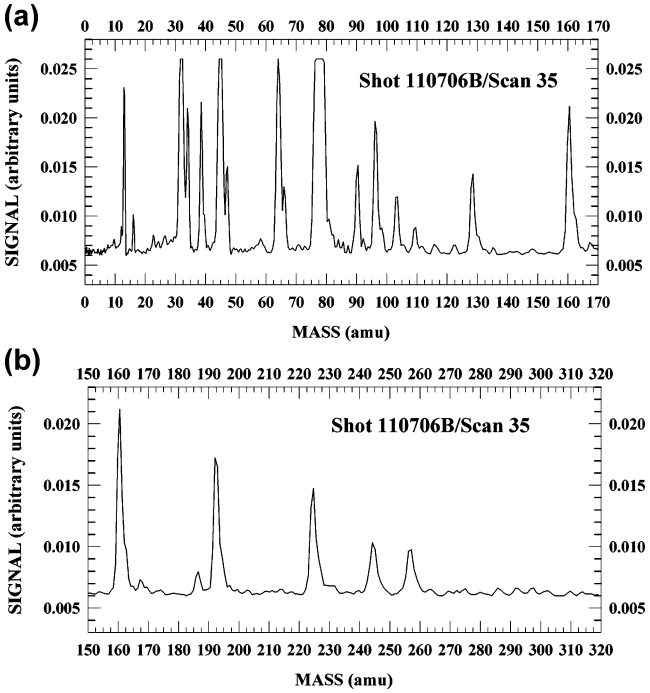

Figure 5. (a) Fragmentation pattern of the chemically reacted liquid $^{13}CS_2$ obtained by shocking the material with 1.80 mass density HMX for the mass range 0−170 amu. (b) Fragmentation pattern of the chemically reacted liquid $^{13}CS_2$ obtained by shocking the material with 1.80 mass density HMX for the mass range 150−320 amu.

TABLE 1: Shocked CS_2 Chemical Species

$^{12}CS_2$ observed masses	possible species	$^{13}CS_2$ observed masses	possible species after $^{13}CS_2$ experiment
32.1	S	32.0	S
44.1	CS	45.1	CS
64.1	S_2	64.1	S_2
76.2	CS_2	77.2	CS_2
88.2	C_2S_2	90.3	C_2S_2
96.3	S_3, C_8	96.3	S_3
100.4	C_3S_2	103.3	C_3S_2
108.3	CS_3,C_6S	109.4	CS_3
112.3	C_4S_2	116.2	C_4S_2
128.3	S_4,C_8S	128.3	S_4
160.4	S_5,C_8S_2	160.4	S_5
184.4	C_2S_5,C_7S_3	186.3	C_2S_5
192.4	S_6,C_8S_3	192.4	S_6
224.7	S_7,C_8S_4,$C_{16}S$	224.4	S_7
240.7	C_{20},C_4S_6,$C_{12}S_3$	244.5	C_4S_6
256.7	S_8,C_8S_5,$C_{16}S_2$	256.5	S_8
297.1	C_6S_7,$C_{14}S_4$,$C_{22}S$	??	C_6S_7,$C_{14}S_4$,$C_{22}S$

A 20-point running average has been used to smooth the raw data.

There is still ambiguity for the structure with mass 297.1 amu. We were never able to see this peak in the $^{13}CS_2$ experiments. It is possible this peak actually corresponds to more than one atomic composition and, therefore, goes below our detectability when the two or three structures are fragmented. Given the carbon composition of the other observe species, it is probably C_6S_7.

The sulfur clustering observed in the experiments is striking. We see the whole sequence of sulfur clusters from S_2 to S_8. Another interesting sequence is C_2S_2, C_3S_2, and C_4S_2.

Scans just preceding the scans discussed above show a strong "loading up" of the S and S_2 lines during the chemical reactions. The change in the strength of the S_2 line is particularly pronounced as it is barely visible in the fragmentation pattern of CS_2 (see Figure 3). The intensity behavior of the S_2^+ line, in particular, presages the appearance of the heavy sulfur products, becoming larger than the CS_2^+ parent line when the heavy sulfur products appear. This leads us to conclude that the less massive S_n structures need to be formed before the more massive ones can appear.

IV. Computed Fluid−Mechanical Results

The CTH wave propagation code[9] was chosen to do the fluid−dynamical modeling of the experiments. CTH is a mixed Eulerian/Lagrangian code; i.e., the problem is set up in the Eulerian frame and then mapped to the Lagrangian frame, where the fluid motion is calculated for one time step. The results are then mapped back into the Eulerian frame. This process is repeated for each time step. This methodology eliminates some of the problems associated with cell distortion experienced with pure Lagrangian codes. This code has been used previously to model other similar types of high explosive mass spectroscopy experiments.[10,11] Details relating to the high explosive burn models used in CTH code are discussed in these references.

All the calculations were done in two-dimensional cylindrical geometry with the problem set up as close as possible to that shown in Figure 2. A Kapton flyer traveling 4.9 mm/μs impacted either pressed HMX or HNS, which then detonated and drove a shock into the CS_2 liquid. The shockwave attenuated as it traveled through the CS_2 liquid, as shown in Figure 6.

Since the wave input into the CS_2 is not flat-topped, the CS_2 at any given Lagrangian position experiences a different pressure vs time history. For example, the CS_2 nearest the spectrometer is shocked and then released immediately, while the material in the center of the cell is shocked to a high pressure and then released by the following rarefaction (produced by the Taylor (rarefaction) wave in the detonating explosive[13]) to a low value before it is completely released by the free surface rarefaction. The times that the shock moved into and out of the CS_2 and also the pressures experienced by the CS_2 at these times are given in Table 2.

In the case of the HMX-driven experiments, the CS_2 input pressure is ca. 180 kbar, which is reduced to 110 kbar by the following rarefaction wave. For the HNS-driven experiments, the pressures are less by 10 and 35 kbar, respectively.

Temperature calculations were also done to get an idea of the temperatures present in the shocked CS_2. These temperatures should only be taken as estimates because the CS_2 equation of state used in the CTH code is not considered capable of predicting accurate temperatures. The data from these calculations are shown in Figure 7 at three times (positions) in the CS_2. The same type of attenuation that occurs in pressure also occurs in the temperature.

The HMX-driven CS_2 shock input temperature was ca. 3500 K and was attenuated to about 1900 K; the HNS-driven CS_2 temperatures were down by about 500 K. These values represent the conditions at Lagrangian positions along the symmetry axis of the cylinder. These are the conditions that the CS_2 experienced before being released by the rarefaction from the free surface. It is apparent from Figures 6 and 7 that the pressure and temperature were held up for a period of time before being released by the rarefactions. The material at the middle Lagrangian position was held up for over 150 ns, while the material at the Lagrangian position near the front of the CS_2 sample was released immediately. It is also interesting to note that the residual temperature of the CS_2 is about 100−200 K

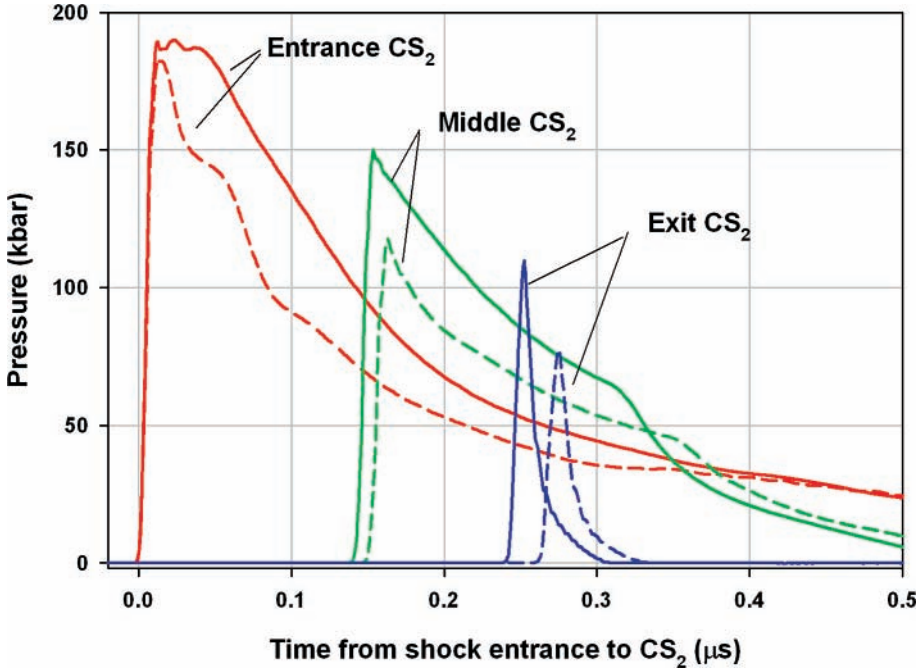

Figure 6. Calculated shock pressure profiles at three Lagrangian positions in the CS_2: (1) at the entrance (red), (2) in the middle (green), and (3) near the exit (blue). The solid line profiles are for the HMX-driven experiments, and the dashed lines are those for the HNS-driven experiments. These Lagrangian points are all along the symmetry axis of the cell.

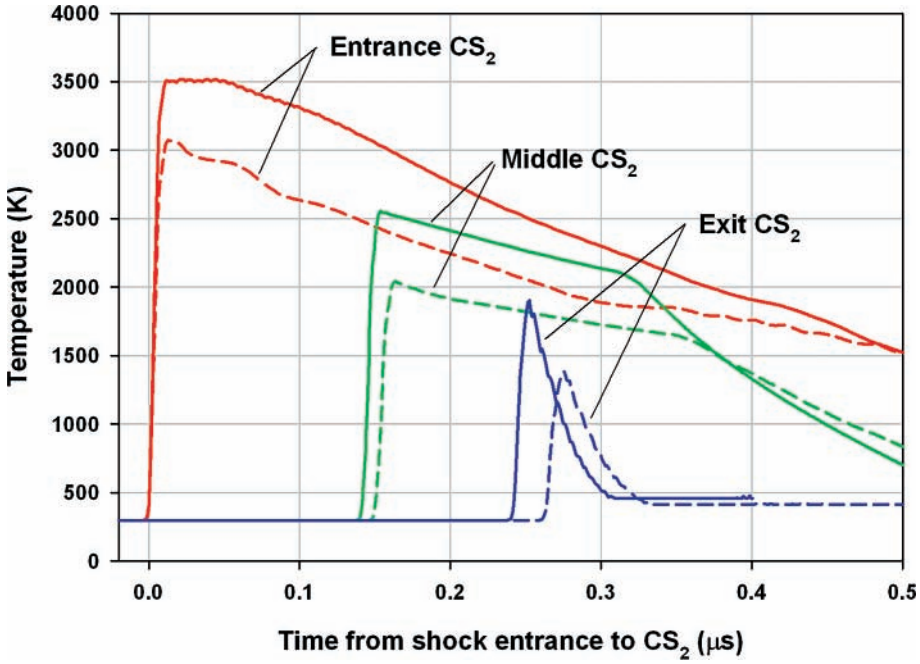

Figure 7. Calculated shock temperature profiles at three Lagrangian positions in the CS_2: (1) at the entrance (red), (2) in the middle (green), and (3) near the exit (blue). The solid line profiles are for the HMX-driven experiments, and the dashed lines are those for the HNS-driven experiments. These Lagrangian points are the same as those in Figure 6.

TABLE 2: Shock Information Derived from CTH Calculations

HE driver material and density (g/cm^3)	time for shock into CS_2 (μs)	time for shock exit CS_2 (μs)	CS_2 shock pressure entrance (kbar)	CS_2 shock pressure exit (kbar)	CS_2 shock temperature entrance (K)	CS_2 shock temperature exit (K)	free surface speed of CS_2 (mm/μs)
HMX 1.80	0.36	0.62	180	110	3500	1900	~4.0
HNS 1.60	0.47	0.75	170	75	3000	1400	~3.1

above ambient; i.e., it is not reduced completely to ambient temperature by the rarefactions due to the irreversibility produced by the shockwaves.

There are two-dimensional effects that come into these experiments as a result of the different shock impedances of the various materials involved in the experimental setup. These effects are shown graphically in Figure 8 at various times during the experiments. Figure 8 shows snapshots of when the HE-driven shock initially reaches the CS_2, when it is in the middle of the CS_2, when it exits the CS_2, and two later times.

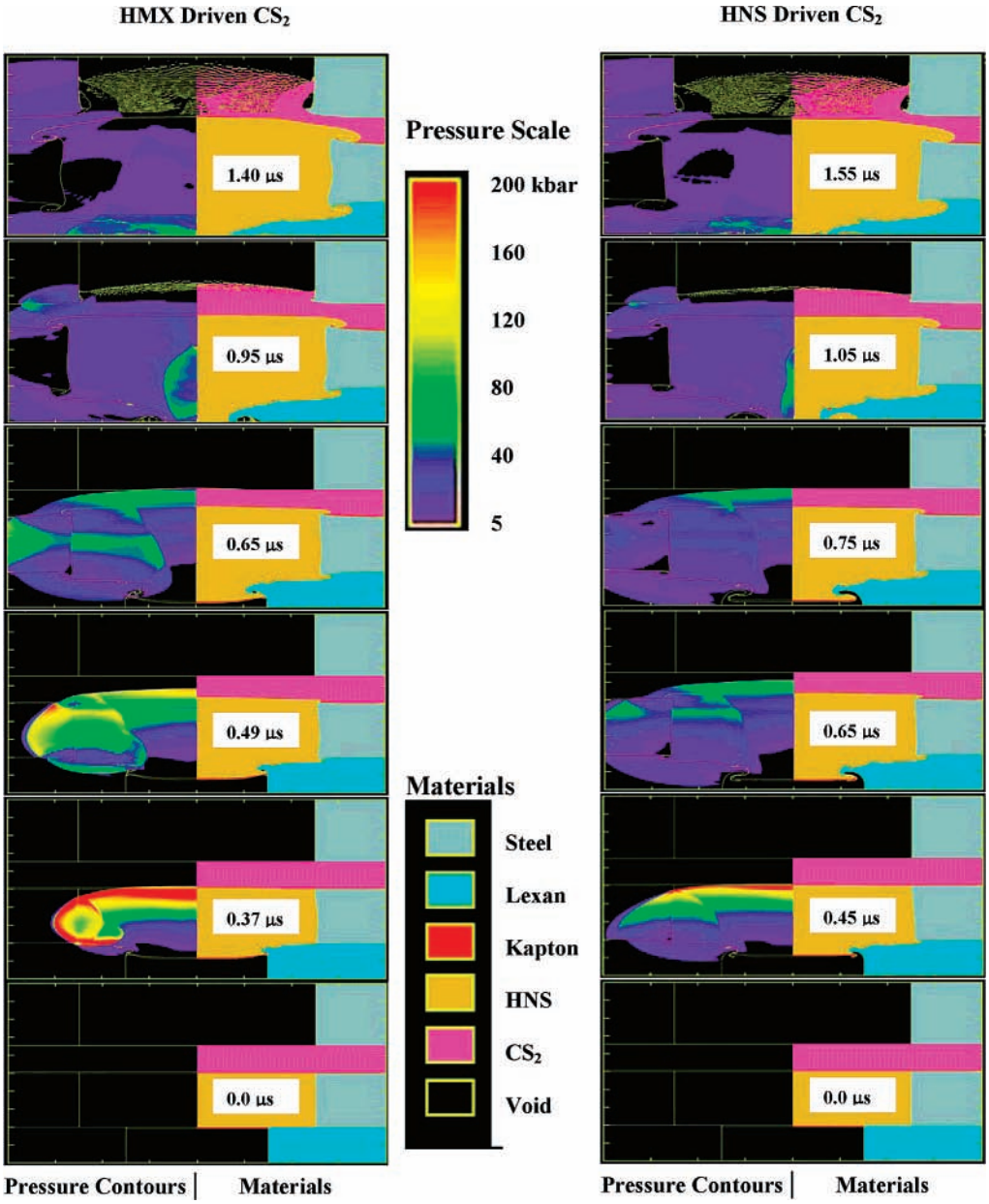

Figure 8. Two-dimensional pressure/material snapshots of the cell at particular times in the calculations. The line that divides a time snapshot between the pressure and material displays is the center line (i.e., the symmetry axis) of the experiment. The reader should note that this figure only displays a portion of the shot assembly and that the length units on the *x* and *y* axes are not equal. At the time equals zero frame, the right side of the explosive is 2.5 mm from the cell center line, and the CS_2 sample thickness is 1.52 mm. The left side series is for the HMX-driven experiments, and the right side is for the HNS-driven experiments. The times are different because of the difference in the detonation and shockwave speeds in the two types of experiments. The bottom picture is at the initial condition, and there is a progression of times moving upward from the bottom: (1) shock front enters the CS_2; (2) shock front in the middle of the CS_2; (3) just before the shock front exits the CS_2; (4) free surface is moving out and starts to spall; and (5) later when considerable spall has taken place. A pressure scale is shown to help estimate the pressure on the left side of each picture and the materials are colored differently on the right so it is possible to see how they evolve with time. Interfaces are also shown in each picture.

There is a difference in times between the HMX-driven and the HNS-driven experiments because the HMX has a higher detonation speed. The HMX also drives a higher-pressure shock into the CS_2, making the shock speed in the liquid higher than in the case of the HNS-driven experiments. At the last time frame in Figure 8 (for both calculations), the phenomena in the HNS lag behind those of the HMX by over 0.15 μs. From Table 2, the free surface speed of the liquid is about 4 mm/μs for the HMX-driven material and 3.1 mm/μs for the HNS-driven material.

The final time shown in Figure 8 for each calculation shows a large amount of "spall" in the liquid as it moves out into the vacuum. CS_2 has a low tensile strength, so as the various waves interact, this type of breakup would be expected. This is mirrored in the mass spectrometry results, which show the material arriving as separate layers.

It is appropriate to examine some general features of the CS_2 flow as shown quantitatively on Figure 8. The material that reaches the mass spectrometer only comes from a small region near the center line of the CS_2 sample. As the sample exits the steel "top" of the cell, a rapid lateral expansion occurs due to the pressure gradient across the sample. This causes the number density of the material reaching the spectrometer to rapidly decrease. This limits one's ability to look deep within the sample. As noted above, the sample near the front of the cell essentially immediately rarefies to near-ambient conditions due

to the rarefaction arriving from the front of the cell. Clearly, no significant chemical kinetics can occur in this portion of the sample. This is mirrored in the experiments since many scans of CS_2 are seen before we begin to see reaction products. We only see heavy reaction products from material deeper within the sample and then only for a few scans due to these two effects: that is, (1) the lateral expansion of the sample that decreases the number density of material reaching the spectrometer and (2) the front rarefaction wave that quenches the chemical kinetics for CS_2 near the front of the sample. An additional factor that decreases our ability to see the reaction products is that the electron beam that ionizes the neutral molecular beam is only on for ca. 8% of the time (i.e., 1 μs every 12 μs). Hence, species only fleetingly present can be missed. After exiting the cell, the free expansion of the sample to the free-molecule phase imparts a considerable speed to the molecules. The sample in the HMX experiments that arrives earliest at the detectors has a speed of ca. 8 mm/μs (before it is ionized). At scan 46, the molecules with mass 256.7 have a speed of 2.3 mm/μs and a kinetic energy of 6.8 eV (before being ionized).

V. Discussion and Conclusions

As noted earlier, the fractional decrease in volume between the two cusps on the CS_2 Hugoniot is approximately −26%. It is of interest to compare this value with the fractional decrease in volume that occurs when CS_2 is frozen. Bridgman's Figure 7 in ref 1b is a graph of the fractional change in volume of CS_2 upon freezing at various pressures. This graph can be extrapolated to ambient pressure, and it gives a fractional volume change of ca. −5.3% upon freezing. Another interesting value is the fractional volume change at his highest pressure (ca. 35 kbar), which is −2.4%. Note that the first cusp on the CS_2 Hugoniot is at ca. 50 kbar. Thus, the change in volume between the two Hugoniot cusp points is more than 10 times larger than the contraction upon freezing in the vicinity of the first cusp. The volume change between the two cusp points is much larger than the volume change in the liquid to solid phase change.

We found 13 species heavier than CS_2. All these species have masses less than 300 amu. It is of interest to determine how many structures of the form C_mS_n can be formed with mass less than 300 amu. Such structures must obey the inequality

$$12m + 32n \leq 300 \quad (1)$$

where m and n are positive integers or zero. There are 136 solutions of inequality (eq 1); of the 136 solutions, 12 have mass ≤76 amu. Therefore, there are 124 possible structures with the possible atomic compositions. We observed approximately 10% of all the possible stoichiometries in our experiments.

Next we relate our observations to the work of other observers. Our treatment is not exhaustive. We limit our discussion to experimental papers done on CS_2 in its condensed phases.

Butcher et al. generated an experimental pressure−temperature ($P-T$) phase diagram for CS_2 using static high-pressure techniques.[14] For temperatures greater than ca. 300 °C, they found a "decomposition region" for all the pressures they examined greater than 25 kbar. They speculated that this region corresponds to the formation of material composed of carbon and sulfur (clusters?). They found that the $P-T$ region in which "Bridgman black" exists is quite restricted.

Agnew et al.[15] gave a somewhat modified version of CS_2's $P-T$ diagram that they obtained using diamond−anvil cell techniques. They used infrared absorption to identify molecular species; a larger area in CS_2's $P-T$ plane was covered in their experiments than in refs 1 and 14. Five molecular species were observed. These were: (1) Bridgman black, (2) C_2S_4 (a chemically bound dimer of CS_2), (3) a $(C_2S_3)_n$ polymer, and (4) and (5) two species they were unable to identify. Their experiments were done on material held at pressure for as long as several hours. As can be seen from Table 1, only the C_4S_6 structure is common to our observations and those in ref 15. Perhaps we are seeing the beginning of the formation of the $(C_2S_3)_n$ polymer they suggest is present. It should be noted that the carbon sulfide C_4S_6 is sufficiently stable for cyclic forms of the molecules to be studied crystalographically. The crystal structures of two isomers of the molecule are known.[16]

Detectable amounts of C_3S_2, S_6, S_7, and S_8 have been found in pure liquid CS_2 subjected to ultrasound of 20-kHz frequency.[17] High pressures are achieved in ultrasound experiments by the collapse of cavitation bubbles produced by the sound waves. Similar observations of C_3S_2 have been made by Cataldo and Heymann.[18] Other workers have detected C_2S_2 and C_3S_2 neutrals and radical cations via mass spectroscopic methodologies.[19] We also see these species. Sulzle et al. have observed C_4S_2.[20] Gerbaux et al., via electron-impact ionization experiments, have detected the CS_3 and C_2S_2 compositions and their radical cations.[21] We also found these species.

It is clear from Table 1 that the shock chemistry induced in CS_2 is complex and involves many different kinetics steps. Table 2 shows that the induced chemistry is a strong function of the shockwave strength. We saw no new chemical species when liquid CS_2 was shocked to over 75 kbar for ca. 0.28 μs. But when a shockwave with strength greater than 110 kbar was present for ca. 0.25 μs, 13 new species heavier than CS_2 were observed. Another interesting feature of our data is that we see none of the oligomers of the "Bridgman black" polymer; i.e., C_2S_4, C_3S_6, C_4S_8, etc. This fact probably calls into question Dick's[4] hypothesis that the material on the upper branch of CS_2's Hugoniot is pure "Bridgman black" since his experiments and ours were done in the same time regime.

The data in the right-most column of Table 1 should be useful to chemical kineticists, since it is necessary to know both reactant and products before endeavoring to determine the underlying chemical kinetics. It is interesting that in all the experimental papers we cite there is only one suggestion of a kinetic step leading to the chemical species observed: $CS_2 \rightarrow CS + S$. Clearly, determining the kinetics schemes leading to the 13 heavy compositions we have observed is an unexplored field.

The data in Figure 1 can be used to help define the physical states that produce the observed kinetics. One can determine the amount of energy per CS_2 molecule that is delivered by the chemistry-inducing shock to the CS_2 liquid. The change in specific internal energy caused by the passage of a shockwave is given by

$$\Delta E = \frac{1}{2} P(v_o - v) \quad (2)$$

where P is the shock pressure and v_o and v are the initial and shocked material specific volumes.[13] To obtain eq 2, one must assume that the shocked material is an inviscid fluid and that the initial pressure is negligible. With these assumptions, one needs only the mass, momentum, and energy conservation laws to obtain it. Note that no assumption of thermodynamic equilibrium in the shocked fluid is necessary. To obtain the internal energy change per molecule in electron-volts, one must multiply the right side of eq 2 by $1.04 \times 10^{-2}x$ (the molecular

weight of the material being shocked); the units of P are GPa and of υ are cm^3/g. Evaluating eq 2 with the data on Figure 1 shows that the energy delivered by the shock per CS_2 molecule is 0.53 (12.2) and 0.92 (21.2) eV/molecule (kcal/mol) at the first and second cusps on CS_2's Hugoniot, respectively. Thus, the transition states of the initial kinetic steps that lead to the product molecules would seem to be necessarily of low energy. Note that the first intermediate species may be able to contribute chemical energy to the flow since CS_2 is metastable to the elements (with a heat of formation of +27.6 kcal/mol). Also since the system immediately after shock passage is not in thermodynamic equilibrium, the energy contributed by the shockwave may be concentrated in a small number of very high kinetic energy molecules; this would, no doubt, speed up the initial kinetic processes.

Since the shocked system is highly compressed, another factor that must be considered in chemical kinetic studies will have to be whether the volumes of activation and reaction of the chemical intermediates and products play an important part in what processes occur. A simple calculation that assumes the molecular centers of mass lie on a simple cubic lattice allows one to get a gauge of the compression produced by the shockwaves. At ambient conditions, one finds that the molecules occupy cubical boxes with a side length of 4.64 Å. At the first cusp on Figure 1, the box side length has been reduced to 4.04 Å, and at the second cusp the length is 3.68 Å. As a reference, the length of an isolated CS_2 molecule is 3.11 Å, and this length ignores the Van de Waals radii of the sulfur atoms.[22] This indicates that the first kinetics routes that should be studied are those with large negative volumes of activation (ΔV^*). Such kinetics routes are those involving bond formation and ionization reactions which typically have ΔV^* values of −10 and −20 cm^3/mol, respectively.[23] Such reactions are strongly pressure enhanced. It is to be noted that bond cleavage reactions (e.g., $CS_2 \rightarrow CS + S$) are strongly pressure inhibited (with $\Delta V^* =$ ca. +10 cm^3/mol) and, thus, are unlikely to be involved in the initial kinetic steps. One can generate hypothetical reaction schemes that do not involve radical producing processes and that would be pressure accelerated. One such scheme is

$$S{=}C{=}S + S{=}C{=}S \rightarrow S{=}C{=}C{=}S + S_2$$

$$S_2 + S_2 \rightarrow S_4$$

$$S_2 + S_4 \rightarrow S_6$$

$$S_4 + S_4 \rightarrow S_8$$

None of these steps require radical formation by unimolecular bond breaking. The first step (a bond re-ordering) is probably approximately pressure neutral and the three sulfur reactions would be strongly pressure accelerated (two moles of reactants transforming to one mole of products). This reaction scheme produces five of the molecular species seen in our experiments. Any such scheme must be viewed as a speculation until further experimental and theoretical evidence has been developed.

The above discussion suggests that theoretical chemical kineticists should concentrate their efforts on chemical intermediates that are charged species and/or on reactions involving bond formation (e.g., condensation reactions).

References and Notes

(1) (a) Bridgman, P. W. *J. Appl. Phys.* **1941**, *12*, 466. (b) Bridgman, P. W. *Proc. Am. Acad. Arts Sci. (Daedalus*) **1942**, *74*, 399.
(2) Whalley, E. *Can. J. Phys.* **1960**, *38*, 2105.
(3) Dick, R. D. Los Alamos Scientific Lab. Report LA-3915, 1968.
(4) Dick, R. D. *J. Chem. Phys.* **1970**, *52*, 6021.
(5) Sheffield, S. A. *J. Chem. Phys.* **1984**, *81*, 3048.
(6) Sheffield, S. A. *Shock Waves in Condensed Media*; Schmidt, S. C., Holmes, N. C., Eds.; Elsevier Science Publishers: 1988; p 463.
(7) Sheffield, S. A.; Duvall, G. E. *J. Chem. Phys.* **1983**, *79*, 1981.
(8) Blais, N. C.; Fry, H. A.; Greiner, N. R. *Rev. Sci. Instrum.* **1993**, *64*, 174.
(9) McGlaun, M. C.; Thompson, S. L.; Kmetyk, L. N.; Elrich, M. G. Sandia National Laboratories, SAND89-0607, 1989.
(10) Blais, N. C.; Engelke, R.; Sheffield *J. Phys. Chem. A* **1997**, *101*, 8285.
(11) Engelke, R.; Blais, N. C.; Sheffield, S. A.; Sander, R. K. *J. Phys. Chem. A* **2001**, *105*, 6955.
(12) NIST Chemistry WebBook (http:webbook.nist.gov/chemistry).
(13) Engelke, R.; Sheffield, S. A. *Encycl. Appl. Phys.* **1993**, *6*, 327.
(14) Butcher, E. G.; Alsop, M.; Weston, J. A.; Gebbie, H. A. *Nature* **1963**, *199*, 756.
(15) Agnew, S. F.; Mischke, R. E.; Swanson, B. I. *J. Phys. Chem.* **1988**, *92*, 4201.
(16) Beck, J.; Daniels, J.; Roloff, A.; Wagner, N. *Dalton Trans.* **2006**, 1174.
(17) Quellhorst, H.; Binnewies, M. *Z. Anorg. Allg. Chem.* **1996**, *622*, 259.
(18) Cataldo, F.; Heymann, D. *Eur. J. Solid State Inorg. Chem.* **1998**, *35*, 619.
(19) Wong, M. W.; Wentrup, C.; Flammang, R. *J. Phys. Chem.* **1995**, *99*, 16849.
(20) Sulzle, D.; Beye, N.; Fanghanel, E.; Schwarz, H. *Chem. Ber.* **1990**, *123*, 2069.
(21) Gerbaux, P.; Haverbeke, Y.; Flammang, R.; Wong, M. W.; Wentrup, C. *J. Phys. Chem. A* **1997**, *101*, 6970.
(22) Herzberg, G. *Electronic Spectra of Polyatomic Molecules*; Van Nostrand: Princeton, 1967; p 601.
(23) le Noble, W. J. *Prog. Phys. Org. Chem.* **1967**, *5*, 207. (b) Asano, T.; le Noble, W. J. *Chem. Rev.* **1976**, *78*, 407.